Acta Oceanol. Sin., 2019, Vol. 38, No. 11, P. 149–157
https://doi.org/10.1007/s13131-019-1505-4
http://www.hyxb.org.cn
E-mail: hyxbe@263.net

Acoustic sound speed profile inversion based on orthogonal matching pursuit

Qianqian Li[1, 2, 3*], Juan Shi[1], Zhenglin Li[3], Yu Luo[1], Fanlin Yang[1], Kai Zhang[1]

[1] College of Geomrtics, Shandong University of Science and Technology, Qingdao 266590, China

[2] College of Underwater Acoustic Engineering, Harbin Engineering University, Harbin 150001, China

[3] State Key Laboratory of Acoustics, Institute of Acoustics, Chinese Academy of Sciences, Beijing 100190, China

Received 20 June 2018; accepted 15 July 2018

Abstract

The estimation of ocean sound speed profiles (SSPs) requires the inversion of an acoustic field using limited observations. Such inverse problems are underdetermined, and require regularization to ensure physically realistic solutions. The empirical orthonormal function (EOF) is capable of a very large compression of the data set. In this paper, the non-linear response of the sound pressure to SSP is linearized using a first order Taylor expansion, and the pressure is expanded in a sparse domain using EOFs. Since the parameters of the inverse model are sparse, compressive sensing (CS) can help solve such underdetermined problems accurately, efficiently, and with enhanced resolution. Here, the orthogonal matching pursuit (OMP) is used to estimate range-independent acoustic SSPs using the simulated acoustic field. The superior resolution of OMP is demonstrated with the SSP data from the South China Sea experiment. By shortening the duration of the training set, the temporal correlation between EOF and test sets is enhanced, and the accuracy of sound velocity inversion is improved. The SSP estimation error versus depth is calculated, and the 99% confidence interval of error is within ±0.6 m/s. The 82% of mean absolute error (MAE) is less than 1 m/s. It is shown that SSPs can be well estimated using OMP.

Key words: acoustic sound speed, ocean acoustics, compressive sensing, orthogonal matching pursuit

Citation: Li Qianqian, Shi Juan, Li Zhenglin, Luo Yu, Yang Fanlin, Zhang Kai. 2019. Acoustic sound speed profile inversion based on orthogonal matching pursuit. Acta Oceanologica Sinica, 38(11): 149–157, doi: 10.1007/s13131-019-1505-4

1 Introduction

The water sound speed profile and sediment properties have an important impact on the underwater sound propagation, and they determine the sound field characteristics (Li et al., 2015, 2018; Zhang et al., 2016; Yang et al., 2011). For matched-field processing, the estimation of ocean sound speed profiles (SSPs) requires the inversion of an acoustic field using limited observations. Such inverse problems are underdetermined, and require regularization to ensure physically realistic solutions. Tolstoy (Tolstoy, 1992) has indicated that the acoustic fields that have propagated through a range-dependent series of SSPs are identical to those of fields which have propagated through simple range-independent environments given by the average SSP. This linearization avoids the unpredictable stalling of the range-dependent model. And the fewer inversion parameters could effectively reduce the calculation of optimization algorithm. Leblanc (Leblanc and Middleton, 1980) has proved that the empirical orthonormal function (EOF) is capable of a very large compaction of the data set, and the ocean sound velocity profile (SVP) data bank analysis with EOFs provided for a large improvement in the prediction model. However, regularization using EOFs often yields low resolution estimates of ocean SSPs, and the estimated SSP can be highly variable especially when internal waves or currents are strong (Lin et al., 2006; Siderius et al., 2001; Huang et al., 2008; Li et al., 2012). This uncertainty can severely affect the accuracy of inversion for other parameters (Siderius et al., 2001; Huang et al., 2008). Because the EOF has a great relationship with the time and location of the SSP training set, the acquisition of EOF is restricted by SSP completeness and measurement time. In order to improve the accuracy of sound velocity inversion, we have shortened the duration of the training set to enhance the temporal correlation between EOF and test sets.

Since the leading-order EOFs often explain much of the information, the SSP can be expressed by retaining only a few leading-order EOFs. For ocean SSPs, usually no more than 5 EOF coefficients have been used to reconstruct ocean SSPs (Huang et al., 2008). So the SSP is sparse, i.e., few non-zero parameters (out of many) explain the observations, therefore can be compressed. In this paper, the SSPs in range-independent ocean environments are resolved using compressive sensing (CS) (Candès, 2006; Elad, 2010), and the orthogonal matching pursuit (OMP) (Pati et al., 1993) is used as the sparse solver. CS asserts that parameters can be recovered robustly for certain highly underdetermined linear problems via sparse regularization of a least-

Foundation item: The National Natural Science Foundation of China under contract No. 11704225; the Shandong Provincial Natural Science Foundation under contract No. ZR2016AQ23; the State Key Laboratory of Acoustics, Chinese Academy of Sciences under contract No. SKLA201902; the National Key Research and Development Program of China contract No. 2018YFC1405900; the SDUST Research Fund under contract No. 2019TDJH103; the Talent Introduction Plan for Youth Innovation Team in Universities of Shandong Province (Innovation Team of Satellite Positioning and Navigation).

*Corresponding author, E-mail: lqq@mail.ioa.ac.cn

squares cost function, provided that the solutions are sparse (Bianco and Gerstoft, 2016). In ocean acoustics, CS has found several applications in matched field processing (Mantzel et al., 2012; Forero and Baxley, 2014) and beamforming (Edelmann and Gaumond, 2011; Choo and Seong, 2018). As the most common greedy algorithm, the OMP method and a series of improved algorithms are computationally cheaper and converge quickly with less error.

The data set is the temperature and depth (TD) data collected in the South China Sea (SCS). Here, the inversion for SSPs is formulated as an underdetermined linear problem where SSPs are parameterized in a sparse domain using EOFs. In Section 2, EOFs, the OMP algorithm and sparse reconstruction methods are introduced. In Section 3, it is demonstrated that SSPs can be estimated with acceptable error using a few of coefficient. Section 4 is the conclusion.

2 Parameter sparsification and compression reconstruction

2.1 *EOFs and principal component analysis (PCA)*

EOF analysis is capable of a very large compaction of the data set. The method provides a very compact presentation of the total statistical nature of the SSP data bank. EOF analysis can reduce the dimension of continuously sampled SSPs by finding few spatial patterns which explain much of the variance. It is assumed that the SSP matrix is $\boldsymbol{S}$, which are sampled over K discrete points in depth and M instants in time.

$$\boldsymbol{S}=\begin{bmatrix} s_{11} & s_{12} & \cdots & s_{1M} \\ s_{21} & s_{22} & \cdots & s_{2M} \\ \vdots & \vdots & & \vdots \\ s_{K1} & s_{K2} & \cdots & s_{KM} \end{bmatrix}. \tag{1}$$

After averaging the M SSPs, we can get the mean SSP, $\bar{\boldsymbol{s}}=[\bar{s}_1,\bar{s}_2,\cdots,\bar{s}_K]^{\mathrm{T}}$. The mean SSP is subtracted to obtain the residual $\boldsymbol{C}$, i.e., $\boldsymbol{C}=\boldsymbol{S}-\bar{\boldsymbol{S}}$.

$$\boldsymbol{C}=[c_1,\cdots,c_M]\in R^{K\times M}. \tag{2}$$

The PCA method is one of the most widely used data compression algorithms. The data is transformed from the original coordinate system to the new coordinate system. When transforming the coordinate system, take the direction with the largest variance as the coordinate axis direction, because the largest variance of the data gives the most important information of the data. The first new coordinate axis selects the direction with the largest variance in the original data, and the second new coordinate axis selects the direction that is orthogonal to the first new coordinate axis and has the next largest variance. Repeat the process, and the number of repetitions is the dimension of the original data. We find that the latter variances are almost zero. So, we can ignore the rest of the axes, and just keep the first few axes that have the most variance. In fact, this realizes dimensionality reduction to the original data. The singular value decomposition (SVD) selects the matrix composed of eigenvectors with the largest eigenvalue, and can transforms the data matrix into the new space and realize the dimension reduction. So we define the SVD for the matrix $\boldsymbol{C}$ to be

$$\boldsymbol{C}^{\mathrm{T}}=\boldsymbol{U}\boldsymbol{\Sigma}V^{\mathrm{T}}, \tag{3}$$

where $\boldsymbol{V}=[v_1,\cdots,v_K]\in\boldsymbol{R}^{K\times K}$ are eigenvectors of the matrix $\boldsymbol{A}=\boldsymbol{C}\boldsymbol{C}^{\mathrm{T}}\in\boldsymbol{R}^{K\times K}$, and $\boldsymbol{X}=\boldsymbol{U}\boldsymbol{\Sigma}\in\boldsymbol{R}^{M\times K}$ are the coefficients. $\Sigma^2=\mathrm{diag}\left(\left[\lambda_1^2,\cdots,\lambda_K^2\right]\right)\in\boldsymbol{R}^{M\times K}$ and $\boldsymbol{\Omega}=[\lambda_1,\cdots,\lambda_K]$ are the eigenvalues of the matrix $\boldsymbol{A}$. The EOFs v_i with $\lambda_1^2\geqslant\cdots\geqslant\lambda_K^2$ are spatial features of the SSPs which explain the greatest variance of $\boldsymbol{C}$. If $M>K$, $\boldsymbol{V}$ forms a basis in $\boldsymbol{R}^K$.

The percentage of total fit energy is defined as

$$E_i=\frac{\sum_{j=1}^{i}\lambda_j^2}{\mathrm{trace}\left(\Sigma^2\right)}. \tag{4}$$

Thus, it is obvious that the largest eigenvalues are more statistically significant than the smaller values. Moreover, one can extract most of the statistically significant information with several vectors when the eigenvalues diminish rapidly. Further, it can be said that the small eigenvalues are more subject to noise (Leblanc and Middleton, 1980).

2.2 *SSP reconstruction using EOFs*

Since the first few EOFs often explain much of the information in $\boldsymbol{C}$, the SSP can be compressed by retaining only the leading P order EOFs,

$$\widehat{\boldsymbol{S}}^{\mathrm{T}}=\bar{\boldsymbol{S}}^{\mathrm{T}}+\boldsymbol{X}_P\boldsymbol{V}_P^{\mathrm{T}}, \tag{5}$$

where $V_P\in R^{K\times P}$ is the dictionary containing the P leading-order EOFs and $X_P\in R^{M\times P}$ is the dictionary coefficient vector. Since the entries in X_P are orthonormal, the coefficients are solved by

$$\widehat{X}_P=\left(\widehat{S}^{\mathrm{T}}-\bar{S}^{\mathrm{T}}\right)V_P. \tag{6}$$

For ocean SSPs, P usually is no more than 5. And for a K-point discretized ocean SSP,

$$\widehat{c}\,(X)=c_0+\widehat{X}_PV_P^{\mathrm{T}}, \tag{7}$$

where $c_0\in R^K$ is the mean SSP.

2.3 *Sound pressure sparse reconstruction and OMP*

The sound pressure observed from a vertical line array (VLA) of hydrophones in ocean environment is forward-modeled using normal modes (adopting KRAKENC normal mode (Porter, 1992)). Since CS is a technique for finding sparse solutions of underdetermined linear systems, the non-linear response of the forward model to SSP is linearized using a first order Taylor expansion. The pressure $p_{\mathrm{obs}}\in C^{N_r}$ received at an N_r element VLA is modeled by KRAKENC as

$$p_{\mathrm{obs}}=p\,(X)+n, \tag{8}$$

where $p(X)\in C^{N_r}$ is the normal mode propagation given the SSP $c(X)$ and $n\in C^{N_r}$ is Gaussian white noise. Here, the source and the other ocean environments are known and included in the $p(X)$ term.

Slightly perturb the reference SSP, the non-linear response of $p(X)$ to SSP perturbations is linearized using the first order Taylor expansion

$$p\,(X)\approx p\,(0)+\frac{\partial p\,(X)}{\partial X}\,|_{X=0}\,X=p\,(0)+DX, \tag{9}$$

where $p(0)$ is the pressure when the SSP equals to the reference SSP c_0, and the matrix $D=[d_1,\cdots,d_K]\in R^{M\times K}$ contains the differential solution of the N_r pressure observations relative to the K shape function in V. The column d_i is calculated using finite differences, by slightly changing the ith coefficient and keeping the other coefficients at zero.

$$d_i=\lim_{\Delta t\to 0}\frac{p\left(0+\frac{1}{2}\Delta_i\right)-p\left(0-\frac{1}{2}\Delta_i\right)}{\Delta_i}, \tag{10}$$

where $\Delta_i\in R^K$ has one non-zero element in the ith position. Thus, the problem can be seen as an optimization problem for estimation X from observations f,

$$f(X)=p(X)-p(0)=DX. \tag{11}$$

An OMP method (Pati et al., 1993) is a greedy algorithm choosing a waveform that is most approximate the signal in each iteration. Given a collection of vectors $D=\{d_i\}$ in a Hilbert space $\mathcal{H}$, let us define

$$Q=\overline{\mathrm{Span}\{d_n\}},\ \text{and}\ W=Q^{\perp}\ (\text{in}\ \mathcal{H}). \tag{12}$$

D is the dictionary and its vector is d_n, are normalized ($\|d_n\|=1$). Assume the following kth order model ($f\in\mathcal{H}$) is

$$f=\sum_{n=1}^{k}a_n^k d_n+R_k f,\ \text{with}\ \langle R_k f,d_n\rangle=0,\quad n=1,\cdots,k. \tag{13}$$

where f is the current approximation, and $R_k f$ the current residual (error). The superscript k, in the coefficient a_n^k shows the dependence of this coefficient on the model-order. When update this kth-order model to a model of order $k+1$,

$$f=\sum_{n=1}^{k+1}a_n^{k+1}d_n+R_{k+1}f,\ \text{with}\ \langle R_{k+1}f,d_n\rangle=0,\quad n=1,\cdots,k+1. \tag{14}$$

Since elements of the dictionary D are not required to be orthogonal, let,

$$d_{k+1}=\sum_{n=1}^{k}b_n^k d_n+\gamma_k,\ with\ \langle\gamma_k,d_n\rangle=0,\quad n=1,\cdots,k. \tag{15}$$

Thus $\sum_{n=1}^{k}b_n^k d_n=P_{Q_k}d_{k+1}$, and $\gamma_k=P_{Q_k^{\perp}}d_{k+1}$, is the component of d_{k+1} which is unexplained by $\{d_1,\cdots,d_k\}$.

Using the auxiliary model (Eq. (15)), it may be shown that the correct update form the kth-order model to the model of order $k+1$, is given by

$$a_n^{k+1}=a_n^k-\alpha_k b_n^k,\quad n=1,\cdots,k \tag{16}$$

and $a_{k+1}^{k+1}=\alpha_k$, where

$$\alpha_k=\frac{\langle R_k f,d_{k+1}\rangle}{\langle\gamma_k,d_{k+1}\rangle}=\frac{\langle R_k f,d_{k+1}\rangle}{\|\gamma_k\|^2}=\frac{\langle R_k f,d_{k+1}\rangle}{\|d_{k+1}\|^2-\sum_{n=1}^{k}b_n^k\langle x_n,d_{k+1}\rangle}. \tag{17}$$

It also follows that the residual $R_{k+1}f$ satisfies, $R_k f=R_{k+1}f+\alpha_k\gamma_k$, and

$$\|R_k f\|^2=\|R_{k+1}f\|^2+\frac{\|\langle R_k f,d_{k+1}\rangle\|^2}{\|\gamma_k\|^2}. \tag{18}$$

The OMP algorithm is initialed by $R_0 f=f, f_0=0$, and $k=1$. For nonorthogonal dictionaries, OMP will in general converge faster than MP (Mallat and Zhang, 1993). For any finite size dictionary of K elements, OMP converges to the projection onto the span of the dictionary elements in no more than K steps. Furthermore after any finite number of iterations, OMP give the optimal approximation with respect to the selected subset of the dictionary. This is achieved by ensuring full backward orthogonality of the error. The OMP method need to determine the number of non-

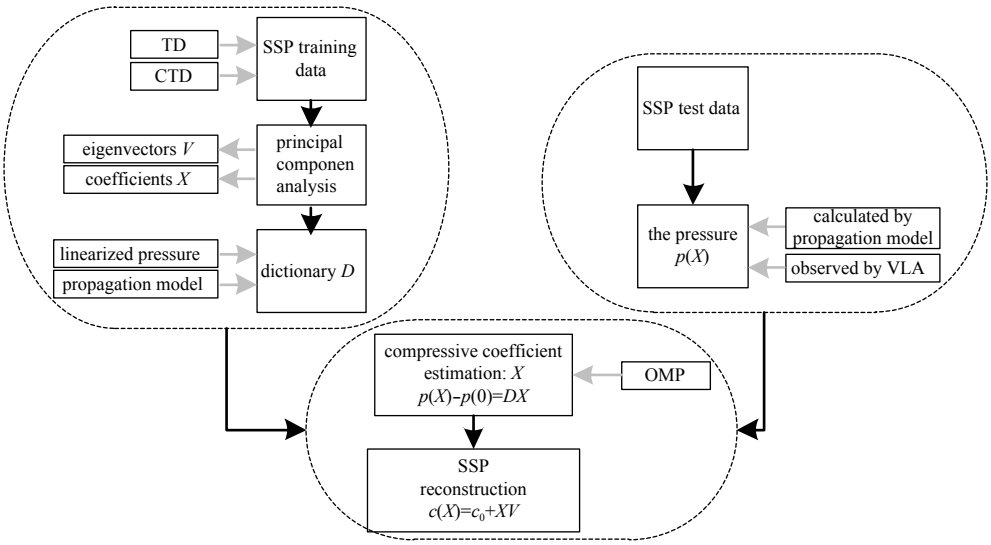

Fig. 1. Flow chart of the experiment process and SSP inversion.

zero elements, according to the EOF method, here, we chose 4 EOFs to represent the SSP. The data processing and parameter inversion process are shown in Fig. 1.

3 Experimental results

The experiment was conducted in September 2015, in the north of the South China Sea. The acoustic source, from the towed sound source at the depth of 40 m, transmitted chirp signals at frequencies between 260 and 360 Hz. A TD survey was conducted during the experiment to provide SSP data and a vertical line array (VLA) was deployed together.

For the waveguide, the water depth is assumed to be the water depth at the TD array for range-independent processing. The seafloor is composed by a halfspace with a density of 2.0 g/cm^3, and a compressional sound speed of 1 800 m/s. The replica field, generated by a 300 Hz acoustic source at 40 m depth, was sampled at 10 km range by N_r evenly spaced VLA elements spanning 2 to 130 m depth, and the attenuation of the basement is 0.1 dB/m.

The SSP data were recorded every 30 s, over a 15 h period, from 23 to 77 m depth, with 3–4 m spacing (20 points). The SSPs are interpolated to K=66 points, with 2 m spacing, and the number of profiles is M=1 750. The SSP data sets are shown in Fig. 2.

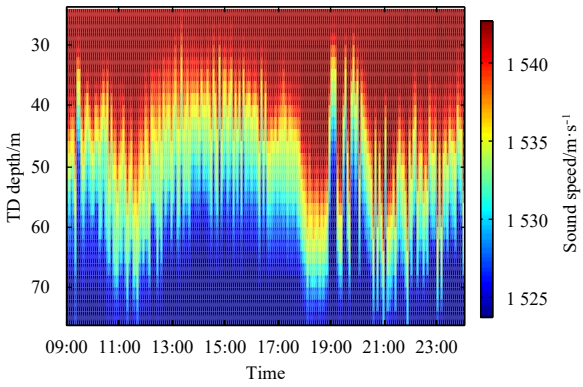

Fig. 2. The sound speed profiles measured by TD chain from 09:00 to 24:00 (GMT), recorded every 30 s.

Considering that the depth range of the TD chain is 23–77 m, and the whole SSP is required to calculate the replica field, isothermal layer expansion can be applied to reconstruct the whole SSP. During the experiment, CTD (conductivity, temperature, and depth) was used once to measure the sea depth, temperature, salinity and sound velocity near the TD chain, from 0.1 to 81.7 m depth, with 0.1 m spacing. According to the salinity information measured by the CTD, the sound velocity can be calculated using the empirical sound speed formula (Chen and Millero, 1977). The full SSP profile data was set as the training set. The SSPs after the reconstruction of the whole sea depth are shown in Fig. 3.

The mean SSP is calculated, and the experimental configuration is shown in Fig. 4.

3.1 *Obtaining EOFs from training data*

The residual sound speed is shown in Fig. 5a, and the max deviation from the mean SSP is more than 10 m/s. EOFs are calculated by the SVD method (Eq. (3)), and Fig. 5b is a plot of the percentage of total fit energy as a function of the number of eigenvectors used. It is apparent that the first few eigenvectors are very effective in the fit. The plot shows that four eigenvector sets of

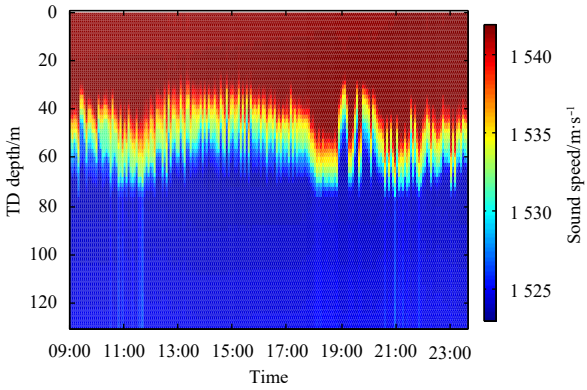

Fig. 3. The whole reconstructed SSPs, recorded every 30 s.

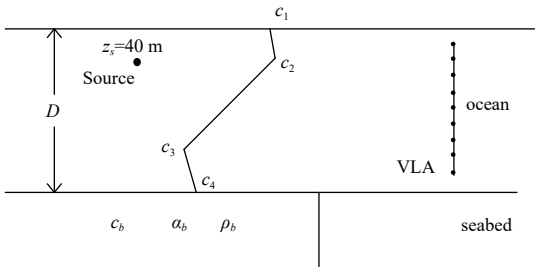

Fig. 4. Experimental configuration and mean SSP.

basis vectors "extract" 97.7% of the data set energy. Figure 5c is a plot of the leading 15-order coefficients for all the SSPs from the training set. It indicates that the coefficients decrease rapidly, and the high-order coefficients are close to zero. The leading order EOFs are shown in Fig. 6. The first eigenvector in Fig. 6 has no zeroes, and it has its largest excursion near the middle of the ocean. Thus, negative thermocline account for most of the energy in the variation in this vector. The second eigenvector has one zero, and the remainder of these plots indicate a behavior like algebraic polynomials—each increase in order being accompanied by an additional zero.

Figure 7 shows the compressed error versus depth for 1 000 randomly SSPs reconstructed by four EOF components. This plot shows the 68% confidence interval (CI), 95% CI, and 99% CI of error respectively from inside to outside. The standard deviation of error (STD) is then

$$\mathrm{STD}\,(z_i) = \frac{\left(1/N_s \sum_{i=1}^{N_s} (c_i - \bar{c})^2\right)^{1/2}}{(N_s)^{1/2}}, \tag{19}$$

where c_i is the compressed sound speed by four EOFs at the depth of z_i (m), and $\bar{c}$ is the mean value of the N_s profiles. The SSP reconstructed error changes versus depth, and the greater error happens in the negative thermocline layer. As shown in Fig. 7, the great reconstructed error by four EOFs is less than 0.1 m/s, which is acceptable.

The coherent matrix for the EOFs in Fig. 8a shows the components in the EOF dictionary are approximately orthogonal. Figure 8b shows the correlation ship between the EOFs and the mean SSP variance in Fig. 6a. We can see that as the order increases, the correlation decreases, and the correlation coefficient decreases rapidly.

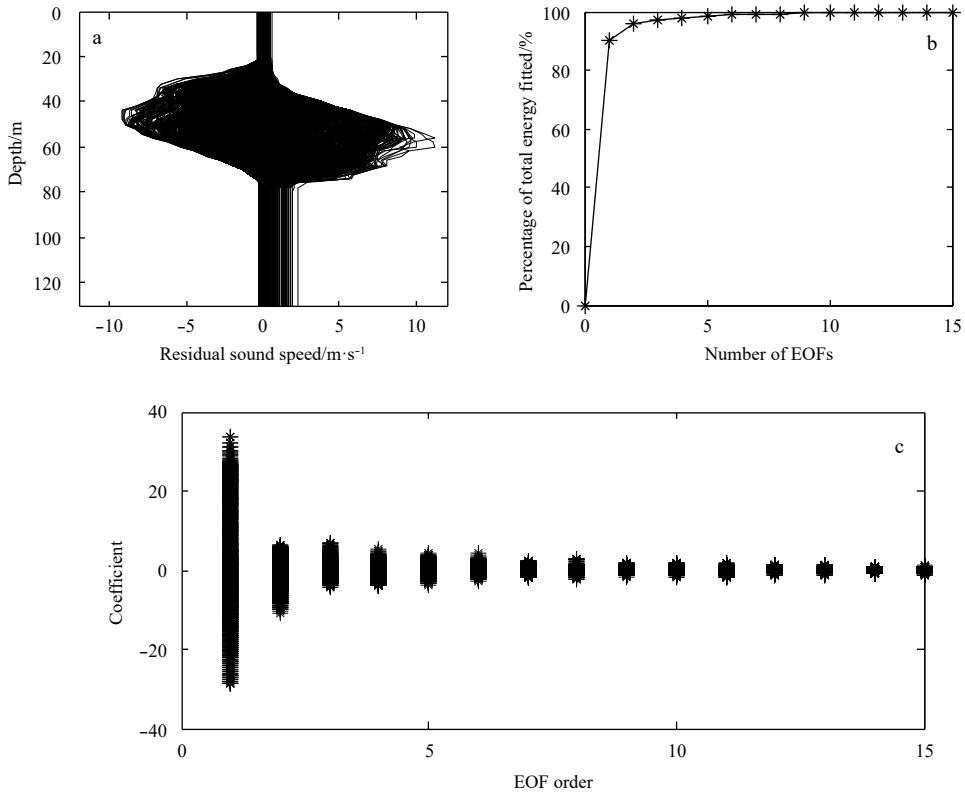

Fig. 5. The EOF method. a. The residual sound speed, b. percent of total energy fitted with limited sets of EOF's, and c. the EOF coefficient.

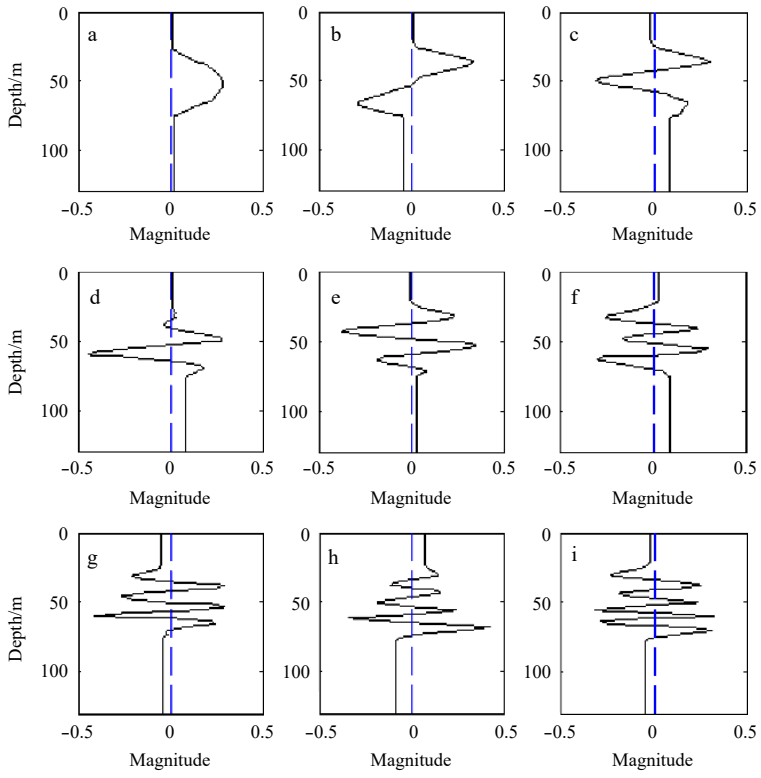

Fig. 6. EOF derived from SSP data.

3.2 *Compressive estimation of SSP*

The performance of OMP is analyzed. It is assumed that the signal is X, and X is a vector with P non-zero coefficients. The length of signal X is K, and the dictionary $D \in R^{N_r \times K}$ is a random

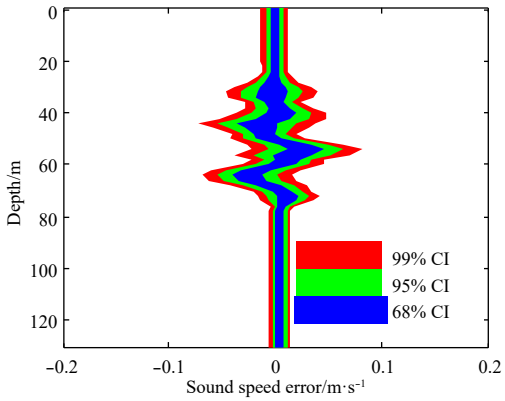

Fig. 7. SSP reconstructed error with 4 EOFs.

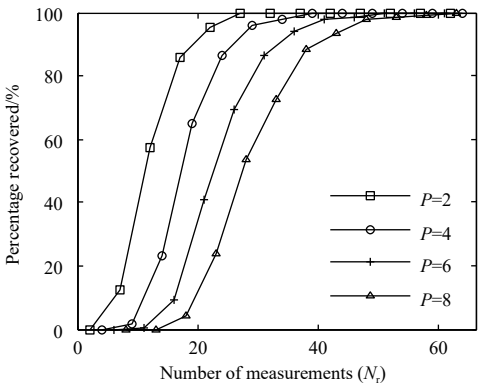

Fig. 9. Percentage of input signals recovered correctly (K=66).

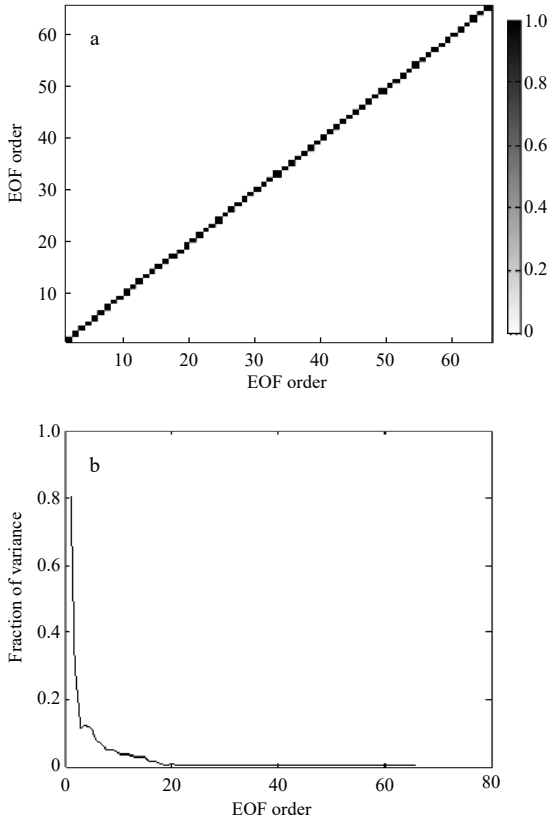

Fig. 8. EOF analysis. a. Coherence of EOFs, and b. fraction of mean SSP variance explained by EOFs.

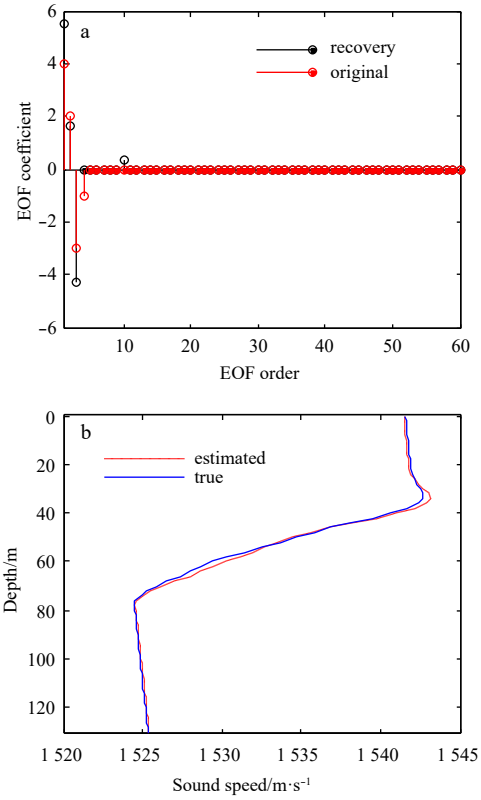

Fig. 10. OMP estimates of four SSP EOF coefficients form noisy observations (SNR=30 dB). a. EOF coefficients, and b. the corresponding SSPs.

Gaussian matrix. The length of the observation vector is N_r, and the sparsity P is set to 2, 4, 6 and 8, separately. For each case OMP is applied to 1 000 realizations (without noise) to allow statistical analysis. The performance is quantified in terms of the probability of correct inversion, defined here as achieving residual errors less than 10^{-6}. Results are given in Fig. 9.

As can be seen from Fig. 9, the larger the sparsity, the larger the number of observations are required to achieve the same accuracy. From the above discussion, it can be seen that the leading 4 EOFs can explain 97.7% of the SSP information. Considering the difficulty brought by increasing the dimension of the observation vector, N_r is set as 29. And the recovery probability is 95.7% in this case (P=4).

Figure 10 shows the estimated SSP with four components (synthetic) with a 30 dB SNR. With one realization of Gaussian white noise, the EOF coefficients are estimated. As shown in Fig. 10, the solution is closed to the true SSP with the max error being 0.9 m/s.

The robustness of the EOF inversion is tested by finding sparse estimates with a 30 dB SNR using a standard deviation metric. The test profiles are selected from the training set one by one. Figure 11a shows the estimated SSPs, and Fig. 11b shows the 68% CI, 95% CI and 99% CI of error respectively from inside to outside. It shows that 99% CI of SSPs error is within 0.8 m/s, and the error in the two isothermal layers is within 0.2 m/s. It also can be seen that the error increases in the negative thermocline layer. This result is consistent with Fig. 7. The main reason is that when

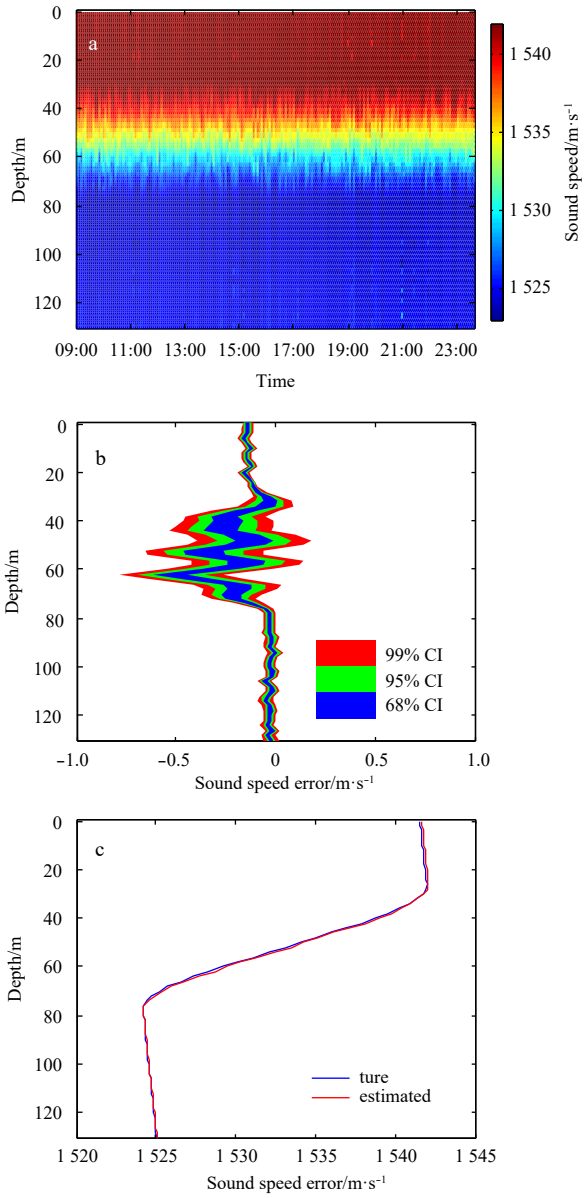

Fig. 11. The estimated SSPs, SNR=30 dB (a) SSP estimation error versus depth (b), and mean SSP (c). Four EOFs are chosen to represent the SSP.

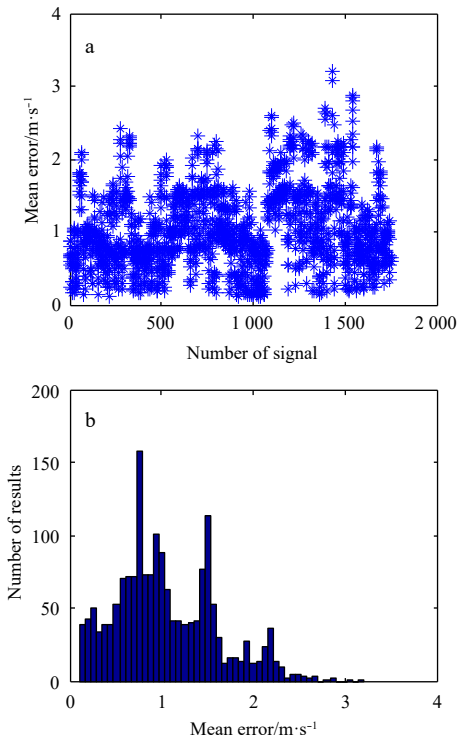

Fig. 12. The mean absolute error of inversion results (a) and distribution of MAE (b).

the first 4 order EOFs are used to reconstruct the sound velocity profile, the SVP loses more information in the negative thermocline layer. Figure 11c shows that the estimated mean SSP is slight larger than the measured mean SSP. This is likely due to the positive numbers are predominate in the first two EOFs (Fig. 6), and it can be seen from Fig. 5c that the coefficient of the first two EOFs have the largest value range, so their weights are the largest. These two reasons make the estimated mean SSP be slightly higher than the measured value. By comparing the citation (Bianco and Gerstoft, 2016), it is found that the OMP algorithm in this paper is more accurate than CVX toolbox.

The mean absolute error (MAE) of all results is shown in Fig. 12a, and the distribution of the MAE is shown in Fig. 12b. It can be seen from Fig. 12 that the MAE of nearly half of the results are less than 1 m/s, and there are still quite a few MAEs between 1 m/s and 2 m/s. Meanwhile, it can be seen from Fig. 11 that the estimated SSP has little fluctuation and fails to reflect the existence of internal waves. This is mainly due to the fact that all 15-h SSPs were used in the calculation of EOFs. Therefore, when the SSP was reconstructed with EOFs, only the average trend during this period was retained. Therefore, we can shorten the length of training set to improve the accuracy of sound velocity inversion.

Figure 13 shows the EOFs trained on shorter SSP training sets (short time span). Here, the SSP training set is a 30 min period. Through the comparison with Fig. 6 (long time span), we find that EOFs change in Fig. 13 are more subtle and higher resolution.

Figure 14a shows the estimated SSPs, and Fig. 14b shows the 68% CI, 95% CI and 99% CI of error respectively from inside to outside. Figure 14a shows that the inverted results are more matched with the measured ones than Fig. 11a. Figure 14b shows that 99% CI of error is within 0.6 m/s, and the error in the two isothermal layers is within 0.1 m/s. It also can be seen that the error increases in the negative thermocline layer. This result is consistent with Fig. 11.

The MAE of all results is shown in Fig. 15a, and the comparison of distribution of the MAE is shown in Fig. 15b. It can be seen from Fig. 15b that MAE peaks around 0 and 0.7 m/s, respectively. Figure 15c shows the cumulative distribution and 82% of the MAEs are less than 1 m/s in the short-time-span method. Obviously, shortening the time span of training set can improve the SSP inversion precision. It shows that proper update of EOF training set can improve the inversion accuracy. The reason is that the EOF has a great relationship with the time and location of the SSP data sets. The acquisition of EOF is restricted by SSP completeness and SSP measurement time. The EOF obtained by

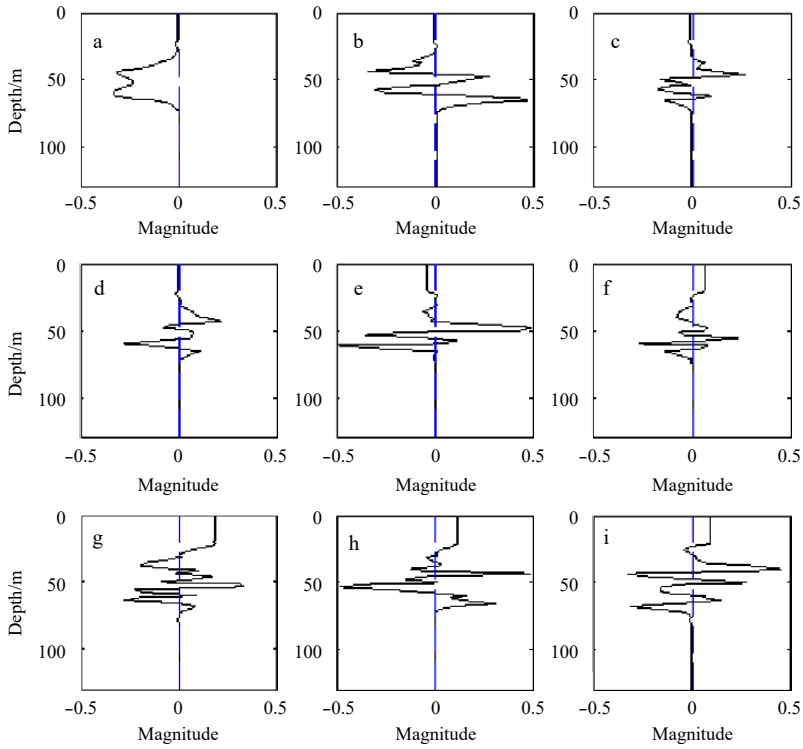

Fig. 13. EOFs derived from one of the shorter SSP training data.

different amounts of SSP data and in different seasons may vary greatly, so the closer the measurement time and position of the SSP training data to the test set, the higher the accuracy of inversion or reconstruction will be.

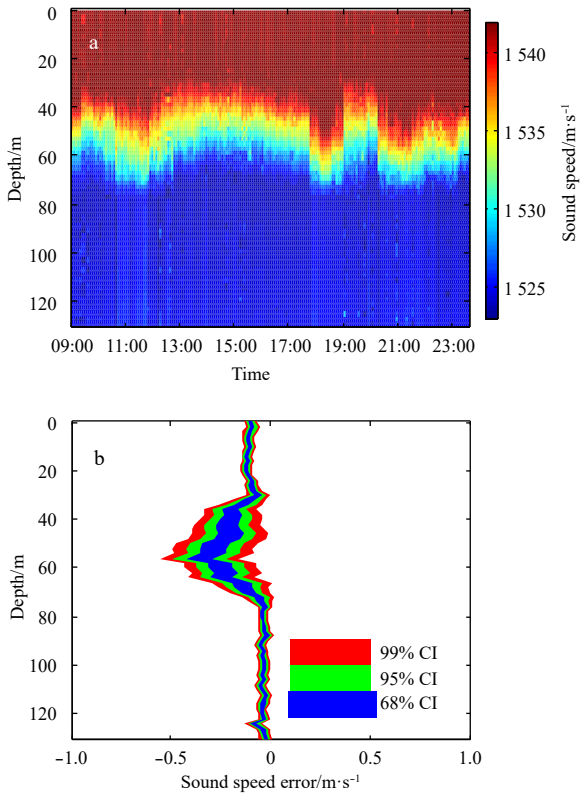

Fig. 14. Short time span. a. The estimated SSPs, SNR=30 dB; and b. SSP estimation error versus depth. Four EOFs are chosen to represent the SSP.

For the short-time-span method, we choose the first 30 min data to study the effect of SNR. The effect of SNR on the mean estimation error is shown in Fig. 16. Figure 16 shows that increasing the SNR will reduce the mean error, that is, the algorithm can break-down if the SNR of the measurements is too low.

4 Conclusions

The pressure observed by VLA is non-linear to SSP, but it can be linearized using a first order Taylor expansion. Since the SSP is sparse, it can be compressed by OMP. It is shown that, with medium SNR, the fine-scale SSP structure is well estimated using OMP. The SVD algorithm is applied to ocean SSP data to calculate EOFs. It is shown that the EOFs trained on a short time span are more subtle and have higher resolution. With proper updated EOFs, the OMP algorithm can further improve SSP inversion resolution with negligible computational expense. This could provide improvements to geoacoustic inversion, matched field processing, and underwater communications.

The restrictive condition of this approach is that the other ocean environments (such as, water depth, array tilt and sediment parameters et al.) needed to know to calculate the matrix $\boldsymbol{D}$. Therefore, the SSP inversion requires good knowledge of the physical properties of the ocean environment. If the environment is not sufficiently accurate, a situation referred to as mismatch, OMP can break down even if the signal-to-noise ratio of the measured signal is high. Therefore, the method in this paper is only applicable to the situation where the other environments are slowly changing and known. However, in most cases, the water depth and sediment characteristics vary with the range and are unknown. In this case, other methods are needed to ensure the accuracy of SSP inversion, such as focalization method (Collins and Kuperman, 1991).

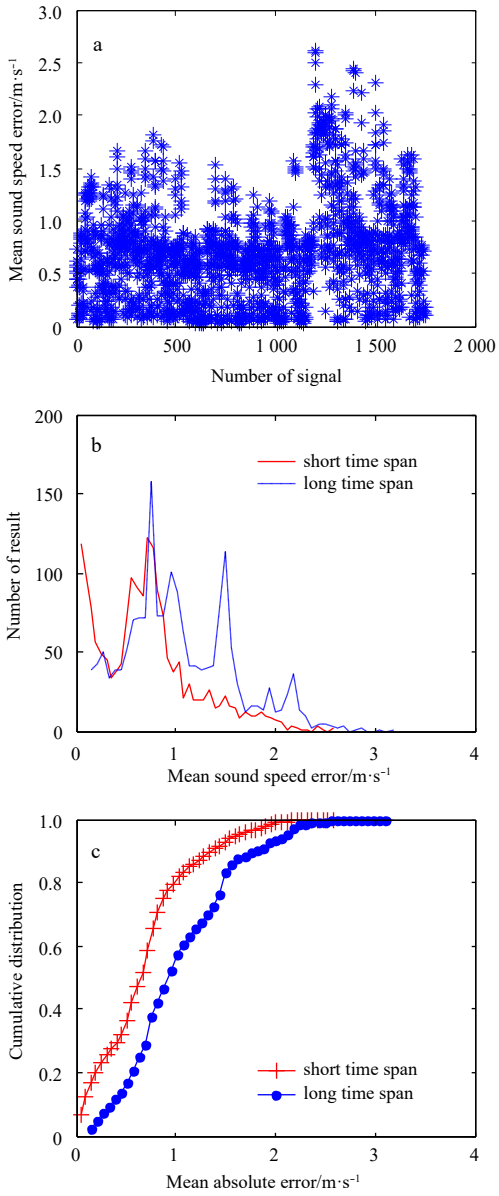

Fig. 15. The MAE of inversion results by short time span (a), comparison of distribution of MAE (b), and comparison of the cumulative distribution (c).

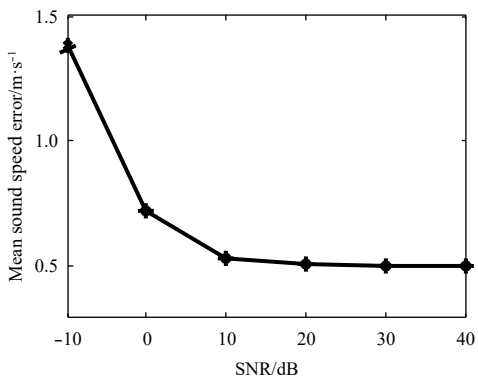

Fig. 16. Mean estimation error versus SNR.

References

Bianco M, Gerstoft P. 2016. Compressive acoustic sound speed profile estimation. The Journal of the Acoustical Society of America, 139(3): EL90–EL94, doi: 10.1121/1.4943784

Candès E J. 2006. Compressive sampling. In: Proceedings of the International Congress of Mathematicians. Madrid, Spain, 1433-1452

Chen C T, Millero F J. 1977. Speed of sound in seawater at high pressures. The Journal of the Acoustical Society of America, 62(5): 1129–1135, doi: 10.1121/1.381646

Choo Y, Seong W. 2018. Compressive sound speed profile inversion using beamforming results. Remote Sensing, 10(5): 704, doi: 10.3390/rs10050704

Collins M D, Kuperman W A. 1991. Focalization: Environmental focusing and source localization. The Journal of the Acoustical Society of America, 90(3): 1410–1422, doi: 10.1121/1.401933

Edelmann G F, Gaumond C F. 2011. Beamforming using compressive sensing. The Journal of the Acoustical Society of America, 130(4): EL232–EL237, doi: 10.1121/1.3632046

Elad M. 2010. Sparse and Redundant Representations. New York: Springer

Forero P A, Baxley P A. 2014. Shallow-water sparsity-cognizant source-location mapping. The Journal of the Acoustical Society of America, 135(6): 3483–3501, doi: 10.1121/1.4874605

Huang Chenfen, Gerstoft P, Hodgkiss W S. 2008. Effect of ocean sound speed uncertainty on matched-field geoacoustic inversion. The Journal of the Acoustical Society of America, 123(6): EL162–EL168, doi: 10.1121/1.2908406

Leblanc L R, Middleton F H. 1980. An underwater acoustic sound velocity data model. The Journal of the Acoustical Society of America, 67(6): 2055–2062, doi: 10.1121/1.384448

Li Zhenglin, He Li, Zhang Renhe, et al. 2015. Sound speed profile inversion using a horizontal line array in shallow water. Science China Physics, Mechanics & Astronomy, 58(1): 1–7

Li Qianqian, Ming Pingshou, Yang Fanlin, et al. 2018. Comparison of two Bayesian-point-estimation methods in multiple-source localization. Acta Oceanologica Sinica, 37(6): 11–17, doi: 10.1007/s13131-018-1215-3

Li Zhenglin, Zhang Renhe, Badiey M, et al. 2012. Arrival time fluctuation of normal modes caused by solitary internal waves. AIP Conference Proceedings, 1495(1): 338–344

Lin Y T, Chen C F, Lynch J F. 2006. An equivalent transform method for evaluating the effect of water-column mismatch on geoacoustic inversion. IEEE Journal of Oceanic Engineering, 31(2): 284–298, doi: 10.1109/JOE.2006.875232

Mallat S G, Zhang Zhifeng. 1993. Matching pursuits with time-frequency dictionaries. IEEE Transactions on Signal Processing, 41(12): 3397–3415, doi: 10.1109/78.258082

Mantzel W, Romberg J, Sabra K. 2012. Compressive matched-field processing. The Journal of the Acoustical Society of America, 132(1): 90–102, doi: 10.1121/1.4728224

Pati Y C, Rezaiifar R, Krishnaprasad P S. 1993. Orthogonal matching pursuit: Recursive function approximation with applications to wavelet decomposition. In: Proceedings of 27th Asilomar Conference on Signals, Systems and Computers. Pacific Grove, CA, USA: IEEE, 40–44

Porter M B. 1992. The KRAKEN normal mode program. Washington D C: Naval Research Laboratory, Report No. NRL/MR/5120-92-6920

Siderius M, Nielsen P L, Sellschopp J, et al. 2001. Experimental study of geo-acoustic inversion uncertainty due to ocean sound-speed fluctuations. The Journal of the Acoustical Society of America, 110(2): 769–778, doi: 10.1121/1.1385898

Tolstoy A. 1992. Linearization of the matched-field processing approach to acoustic tomography. The Journal of the Acoustical Society of America, 91(2): 781–787, doi: 10.1121/1.402538

Yang F L, Lu X S, Li J B, et al. 2011. Precise positioning of underwater static objects without sound speed profile. Marine Geodesy, 34(2): 138–151, doi: 10.1080/01490419.2010.518501

Zhang K, Li Y, Zhao J H, et al. 2016. Underwater navigation based on real-time simultaneous sound speed profile correction. Marine Geodesy, 39(1): 98–111, doi: 10.1080/01490419.2015.1082521